3.45 Term Paper
How to Measure Degree of Spin Polarization
By Lirong Zeng

1   Introduction

1.1 Significance of spin polarization measurement

Spintronics is an emerging field of research combining two traditional branches of physics: magnetism and electronics. It is based on the ability of ferromagnetic materials to conduct spin-polarized currents. The effectiveness of spintronics depends on the extent to which a current is spin-polarized [1], which in turn depends on the spin polarization of the ferromagnetic materials. All device designs improve their performance as the spin polarization P approaches 100%. High degree of spin polarization P is especially important for spin injection experiments where one wants to inject spin polarized current from a ferromagnetic material to a nonmagnetic metal or semiconductor. The P of the source material sets an upper limit to the injection efficiency. Therefore, for both scientific and technological reasons, it is important to be able to measure the degree of spin polarization of a candidate material easily and accurately. This paper introduces four important techniques to measure P, namely spin-resolved photoemission spectroscopy, spin-polarized tunneling in a ferromagnet /insulator/superconductor (FM/I/S) tunnel junction (the Tedrow-Meservy method), measuring tunneling magnetoresistance in a ferromagnet 1/insulator/ferromagnet 2 (FM1/I/FM2) junction, and then calculating P through Julliere's model, and finally, Andreev reflection in a superconducting point contact,. For each method, its principle, experimental setup, relative advantages and disadvantages are discussed.

1.2 Different definitions of spin polarization

Given the growing number of experiments probing P, it becomes increasingly important to calculate P within the framework of the conventional band theory (and eventually beyond it). Spin polarization can be defined in several different ways [2], including, but not limited to, "N"-definition, "Nv^2"-definition and "Nv"-definition. In order to compare calculations with the experimental data, it is crucial to make sure that a proper definition of P is used.

The most natural and popular definition is

$$P = \frac{N_\uparrow - N_\downarrow}{N_\uparrow + N_\downarrow} \qquad (1)$$

where $N_{\uparrow,\downarrow}$ is the density of electronic states (DOS) at the Fermi level, defined as (h/2π is taken as 1)

$$N_i = \frac{1}{(2\pi)^3} \sum_\alpha \int \delta(E_{K\alpha i}) d^3 k = \frac{1}{(2\pi)^3} \sum_\alpha \int \frac{dS_F}{v_{K\alpha i}} \qquad (2)$$

and $E(v)_{K\alpha i}$ is the energy (velocity) of an electron in the band α with spin i ($\uparrow$ or $\downarrow$) and the wave vector K. This definition of P may be called the "N"-definition. A typical experiment that can probe P_N is spin-polarized photoemission. For transport measurements, however, the usefulness of P_N is limited by the fact that usually the transport phenomena are not defined by the DOS alone. This is especially true for materials that have both heavy d-electrons and light s-electrons at the Fermi level (e.g. Ni). In such materials, while the DOS is mostly defined by the heavy d-electrons, the electric transport is primarily due to the fast s-electrons.

Classical Bloch-Boltzmann transport theory can separate the currents of the spin-up electrons and spin-down electrons, and define P via the current densities $J_{\uparrow(\downarrow)}$. Since $J_{\uparrow(\downarrow)} \propto \left\langle Nv^2 \right\rangle_{\uparrow(\downarrow)} \tau_{\uparrow(\downarrow)}$, assuming the same relaxation time τ for both spins, we arrive in the "Nv^2"-definition:

$$P_{Nv^2} = \frac{J_\uparrow - J_\downarrow}{J_\uparrow + J_\downarrow} = \frac{\left\langle Nv^2 \right\rangle_\uparrow - \left\langle Nv^2 \right\rangle_\downarrow}{\left\langle Nv^2 \right\rangle_\uparrow + \left\langle Nv^2 \right\rangle_\downarrow} \qquad (3)$$

Where $\left\langle Nv^2 \right\rangle_{\uparrow(\downarrow)}$ is defined as

$$\left\langle Nv^2 \right\rangle_i = \frac{1}{(2\pi)^3} \sum_\alpha \int v_{K\alpha i}^2 \delta(E_{K\alpha i}) d^3k = \frac{1}{(2\pi)^3} \sum_\alpha \int v_{K\alpha i} dS_F \qquad (4)$$

Unfortunately, it is hardly possibly to measure $J_\uparrow$ and $J_\downarrow$ separately. A typical experiment involves spin-polarized tunneling between a FM and another material. Spin-polarized tunneling is an imbalance in the electric current carried by up- and down-spin electrons tunneling from a ferromagnet through an insulating barrier. Particularly, one can measure tunneling currents separately for both spin polarizations for a ferromagnet/superconductor contact.

Another definition similar to $P_{Nv}{}^2$ is the ballistic definition P_{Nv}, which is applicable to low resistance ballistic contacts. Note that the Nv^2-definition is actually the same as the definition for the spin polarization of a current

$$p = \frac{G_\uparrow - G_\downarrow}{G_\uparrow + G_\downarrow} = \frac{I_\uparrow - I_\downarrow}{I_\uparrow + I_\downarrow} \qquad (5)$$

1.3 What determines P

It is obvious that for the most popular N-definition, the electronic structure at the Fermi level determines P. A typical transition metal has two components to its electronic structure: narrow d bands that may be fully or partially spin-polarized because of the on-site exchange energy, and broad s bands with a lesser degree of spin polarization due to s-d hybridization. Specifically P is controlled by the extent to which these s and d bands cross the Fermi surface [1]. If the orbital character of at the Fermi surface is mainly d-like, then P will be high. On the other hand, if the orbital character is s-like or s-d-hybridized, then P can be low or high depending on the details of the electronic structure. For

different materials, not only the magnitude of P can vary greatly, the sign of P can be positive or negative.

2   Methods to measure degree of spin polarization

Measuring P requires a spectroscopic technique that can discriminate between the spin-up and spin-down electrons near E_F. Four methods to measure P are discussed below, among which the Tedrow-Meservy method is reviewed in most detail because of its wide use and high energy resolution.

2.1 Spin-resolved photoelectron spectroscopy

Spin-resolved photoelectron spectroscopy is technically capable of providing the most direct measurement of P. The first photoemission experiment to observe spin-polarized electrons was conducted on Gd by Busch et al in 1969 [3]. However, in addition to very complicated experimental setup, its energy resolution is hundreds of milli-eV, which is far less than the necessary energy resolution (~1meV) [1].

2.1.1 Principle

Although sometimes ambiguously called spin-resolved photoemission, no photons are emitted in this technique, rather, the "photoemission" actually means photon-induced electron emission. Photoemission may be viewed as a scattering phenomenon by a surface system [4] with (monochromatic) electromagnetic radiation (i.e. photons of energy $h\nu$, momentum $(h/2\pi)\vec{q}$, and a polarization described by the electric field vector $\vec{E}$) in the input channel and electrons (of energy $E' < h\nu$, momentum $(h/2\pi)\vec{k}'$ and the spin polarization vector $\vec{P}$) in the output channel. Fig. 1 depicts the basic mechanism "inside" the system. The photon imparts its energy $h\nu$ to an electron of energy $E_1 < E_F$, exciting it into a previously empty state of energy $E_2 > E_{vac}$. The current associated with the extension of the state E_2 into the vacuum region is then detected as the "photo-current". When the energy of the incident photon is close to the work function of the ferromagnetic metal, only the electrons near the Fermi energy can overcome the vacuum barrier, and they have also to travel perpendicular to the surface in order to escape into the vaccum. Thus with photon energy close to the photothreshold, the initial photoemission state is well-defined.

The dependence of the photoelectron current on the energy, direction and polarization of the incident electro-magnetic radiation, and on the energy and direction of the emitted electrons provides most extensive information on the electronic structure both of the "bulk" solid and of the surface region. Furthermore, by analyzing the spin orientation of the emitted electrons, further and unique insights into the electronic structure of solids and into the photoemission process can be obtained. Spin-polarized photoelectrons can be associated with initial states which have a preferential spin orientation, i.e. the ground state of the system exhibits long-range magnetic order, or associated with spin-orbit

interaction in the initial or the final state (without requiring a direct coupling of the electron spin to the radiation field).

Image removed due to copyright considerations.

Image removed due to copyright considerations.

Fig. 1 Schematic representation of the (valance band) photoemission process (involving the filled vertical line) and its inverse (involving the empty vertical line) in an energy level diagram in the surface region. V_{or} is the real part of the effective potential, and the hatched area indicates the occupied levels (below E_F).

Fig. 2 Schematic of an apparatus for spin-resolved photoemission

2.1.2 Experimental technique

2.1.2.1 Sample preparation

Ferromagnetic samples can be used in their remanent state. To obtain high remanence, the samples have to be shaped suitably with a small demagnetization factor, e.g. thin plates or evaporated films. This kind of samples can be magnetically saturated by applying a short magnetic field pulse of about 200 Oe from a small unsupported coil of a few windings.

Because of the surface sensitivity, the samples have to be atomically clean during the photoemission experiment. Therefore, the apparatus has to be equipped with a surface preparation stage that consists generally of an ion-etching facility and a LEED-Auger system for examining the surface conditions.

2.1.2.2 Light source

Ultraviolet resonance lamps and monochromatized synchrotron radiation in the energy range of 20 to 70 eV or higher can be used as light sources. Due to the tunability and cleanliness (the light emerges from ultrahigh vacuum system), synchrotron radiation is best suited for studying the band dispersions of the highly reactive transition metal surfaces. Energy resolutions of several hundred eV and angle resolution of about $\pm 3^{\circ}$ are achieved.

2.1.2.3 Detector

A conventional photoelectron spectrometer can be used for energy and angle analysis. Spin analysis can be done in different ways. For photoemission from ferromagnetic materials, the Mott detector has been employed. It requires to accelerate the electrons to about 100 keV before scattering on a thin gold foil. Due to spin-orbit coupling, a left-right-asymmetry occurs when the electron beam is spin-polarized perpendicular to the scattering plane.

The left and right count rates N_L and N_R in the Mott detector are accumulated as a function of binding energy, and the spin polarization P(E) can be calculated as

$$P(E) = \frac{1}{S_{eff}} \frac{q(E)-1}{q(E)+1} = \frac{1}{S_{eff}} \frac{N_L - N_R}{N_L + N_R} \qquad (6)$$

where $q = N_L/N_R$. N_L and N_R have to be corrected for the so-called apparatus-asymmetry if $N_L = N_R$ for unpolarized electrons. S_{eff} is the Sherman factor, which can be calculated from scattering theory and corrected for film thickness.

Displaying spin-resolved intensity-energy distribution curves $I^{\uparrow}(E)$ and $I^{\downarrow}(E)$ allows better correlation with the calculated band structures. They are related to the spin polarization P(E) and the spin-averaged intensity I(E) through

$$I^{\uparrow}(E) = 0.5I(E)(1+P(E)) \qquad (7)$$
$$I^{\downarrow}(E) = 0.5I(E)(1-P(E)) \qquad (8)$$

2.1.2.4 Experimental setup

Fig. 2 shows a schematic of the experimental setup which utilizes the well-focused light spot as available with synchrotron radiation. The apparatus is similar when using a high-efficient laboratory resonance lamp.

2.1.3 Advantages and disadvantages

Spin-polarized photoelectron spectroscopy provides the most direct measurement of P as can be seen from the discussion above. Fig. 3 shows the spin-resolved photoemission spectra for a Fe_3O_4 film on a MgO (100) substrate taken with 450 eV photons [4]. However, besides low energy resolution (hundreds of meV), it necessitates complicated apparatus such as synchrotron radiation, and very stringent surface preparation. This makes it not applicable for routine analysis of spin polarization.

Image removed due to
copyright considerations.

Fig. 3 Spin-resolved photoemission spectra of
Fe_3O_4/MgO(100) taken with 450 eV photons [5]

2.2 Spin-polarized tunneling in a FM/I/S tunnel junction-the Tedrow–Meservey method

The pioneering experiments by Tedrow and Meservey [6,7] founded the field of spin-polarized tunneling[8]. They used ferromagnet/insulator/superconductor (FM/I/S) tunnel junctions to measure the spin polarization of the tunneling current originating from various ferromagnetic metals across an Al_2O_3 barrier to a superconducting Al film that acts as a spin analyzer.

2.2.1. Principle

2.2.1.1 General theory of electron tunneling

Electron tunneling is a quantum mechanical phenomenon in which electric current can pass from one electrode through a thin insulating barrier layer into a second electrode. This three-layer system-electrode, barrier, and counterelectrode-is called a tunnel junction. For technical reasons, these junctions have usually been fabricated using a thin metal film (generally Al) as the first electrode, with an oxide providing the barrier. The quantity typically measured in a tunneling experiment is the current or its derivative as a function of applied voltage. With no voltage applied, the Fermi levels of the two electrodes must be equal. An applied voltage will give rise to a difference between the

two Fermi levels. Fermi's golden rule determines the current [7]: the number of electrons tunneling is given by the product of the density of filled states at a given energy in one electrode and the density of empty states in the other electrode at the same energy multiplied by the square of a matrix element describing the probability of tunneling. Usually this matrix element is taken to be independent of energy. Taking the difference between current of tunneling electrons at energy E from electrode 1 to electrode 2 and current from electrode 2 to electrode 1, then integrating over all energies, we get the tunneling current

$$I(V) = |M|^2 \int_{-\infty}^{+\infty} N_1(E - eV)N_2(E)[f(E - eV) - f(E)]dE \qquad (9)$$

where N_1 and N_2 are the densities of states (DOS) of the first and second electrodes, f is the Fermi function, V is the voltage on the first electrode with respect to the second, M is the matrix element, and the energy E is measured from the Fermi energy.

The tunneling case that is relevant for the Tedrow-Meservey method of measuring spin-polarization is when one electrode is superconducting and the other is normal. The BCS superconducting density of states has a gap in the excitation spectrum of Δ on each side of the Fermi level and characteristic singularities in $N_s(E)$ for $E = \pm\Delta$. The BCS superconducting DOS has the form

$$N_s(E) = \begin{cases} (N_n(E)E)/(E^2 - \Delta^2)^{1/2} & |E| \geq \Delta \\ 0 & |E| < \Delta \end{cases} \qquad (10)$$

where N_n is the DOS of the metal in the normal state. For simplicity, the normal state DOS is assumed to be independent of energy and can be removed from the integral in Eq. (9). Thus we arrive at

$$I \sim N_n \int_{-\infty}^{+\infty} N_s(E)[f(E + eV) - f(E)]dE \qquad (11)$$

Little current can flow when $|eV| < \Delta$ since there are only a few thermally filled states on one electrode facing a similar number of empty states in the other. When eV exceeds the gap energy, the current increases rapidly. At higher voltages, the current approaches a linear dependence on V. Taking the derivative of I with respect to V in Eq. (11) leads to

$$\frac{dI}{dV}(V) \sim \int_{-\infty}^{+\infty} N_s(E)K(E + eV)dE \qquad (12)$$

Therefore, dI/dV is the convolution of the superconducting DOS $N_s(E)$ and K(E-eV), the derivative of the Fermi function with respect to V,

$$K = \beta \exp[\beta(E + eV)]/\{1 + \exp[\beta(E + eV)]\}^2 \qquad (13)$$

Here $\beta = 1/KT$. The function K peaks at E=eV and approaches a δ-function as the temperature $T \to 0$. Thus, in the limit of low temperature, the conductance dI/dV(V)

approaches $N_s(eV)$ and a measurement of tunneling conductance closely reflects the density of the excited states of the superconductor. Actually, by a deconvolution, the DOS can (at least in theory) be reconstructed from the conductance data. Fig. 4 manifests the directness and power of this kind of measurement.

Fig. 4 Superconductor-normal metal tunneling. **(a)** BCS density of states of a superconductor as a function of voltage. **(b)** Temperature dependent kernel in the integral expression for the conductance. **(c)** Theoretical normalized conductance dI/dV. Voltage is measured from the Fermi energy of the superconductor. Note that electron energy decreases as the voltage increases.

Fig. 5 (a) Magnetic field splitting of the quasiparticle states into spin-up (dashed) and spin-down (dotted) densities. **(b)** Spin- and temperature-dependent kernel in tunneling conductance integral. **(c)** Spin-up conductance (dashed), spin-down conductance (dotted), and total conductance (solid line).

2.2.1.2   Zeeman splitting of the density of states of a superconductor

Zeeman splitting of the DOS of a superconductor makes it useful as a spin detector.

Generally, in a tunneling experiment in a magnetic field, the orbital deparing parameter of the superconductor dominates and the measured conductance simply reflects a broadening of the DOS with increasing field. However, when a thin superconducting film (a few nanometers or less) is placed in a magnetic field applied parallel to the film plane, the orbital response is largely suppressed, so the effect of the spin interaction with the field can be observed. In this case, the quasiparticle DOS of a superconductor split due to the Zeeman interaction of the magnetic field with the electron spin magnetic moment. The explanation goes as follows: the paired quasiparticles must be in time-reversed states. When the filed is applied, they keep their k↑ and -k↓ paring, but now the spin-up and spin-down members of the pair have different energies, one being raised by $\mu_B H$, and the

other lowered by $\mu_B H$, with μ_B the Bohr magneton. The excited states remain separated from the paired state by Δ, so that in a tunneling experiment, the peaks of the BCS DOS appear at different voltages for quasiparticles of different spin. As a result, the DOS of the superconductor is the superposition of the spin-up and spin-down contributions separated by energy of $2\mu_B H$ (see Fig. 5(a)). This Zeeman splitting of the sharply peaked supercondoctor DOS makes it possible to separate the contributions from the up- and down-spin electrons in the tunneling current, since at an energy of $\Delta - \mu_B H$, the electrons in the tunnel current will be almost entirely of one spin orientation, and at $\Delta + \mu_B H$ almost entirely of the opposite spin direction. So the superconductor in a superconductor/normal metal junction (S/I/N) can be used as a spin analyzer.

In the absence of spin-orbit scattering and orbit deparing, the measured conductance is the sum of that for each spin in the form of Eq. (12):

$$\frac{dI}{dV}(V) \sim \int_{-\infty}^{+\infty} N_s(E + \mu H) K(E + eV) dE + \int_{-\infty}^{+\infty} N_s(E - \mu H) K(E + eV) dE \qquad (14)$$

Fig. 5 demonstrates how the two-peaked structure develops from spin DOS in a way very similar to that described in Fig. 4.

2.2.1.3 Conductance asymmetry of a S/I/FM junction

Let us proceed to see what will happen when a ferromagnet is used as the counterelectrode to the superconducting electrode.

In a ferromagnet, the electronic DOS is exchange split, leading to unequal DOS at the Fermi energy, $N_\uparrow \neq N_\downarrow$. Since $N_\uparrow$ and $N_\downarrow$ determine the number of electrons that can tunnel within each spin channel, the spin conductance is weighted with the respective spin DOS. Neglecting spin-orbit scattering and assuming that spin does not change during the tunneling process, i.e. the total conductance is the sum over the spin-up and spin-down channels, using essentially the same form as Eq. (14), we obtain

$$\frac{dI}{dV}(V) = \sigma(V) \sim \int_{-\infty}^{+\infty} a N_s(E + \mu H) K(E + eV) dE + \int_{-\infty}^{+\infty} (1 - a) N_s(E - \mu H) K(E + eV) dE \quad (15)$$

Here a is the fraction of electrons with magnetic moment in the direction of the applied magnetic field. The spin polarization P of the ferromagnet is then defined as

$$P \equiv \frac{n_\uparrow - n_\downarrow}{n_\uparrow + n_\downarrow} = \frac{Na - N(1 - a)}{N} = 2a - 1 \qquad (16)$$

where N is the total number of electrons in the ferromagnet at the Fermi energy, and $n_\uparrow$ and $n_\downarrow$ are the number of electrons whose magnetic moments are parallel and antiparallel to the field, respectively.

Eq. (15) gives an asymmetric conductance curve as shown in Fig. 6. The dashed curve in Fig. 6(a) shows the spin-up DOS; the dotted curve shows the spin-down one, identical but displaced in energy by $2\mu_B H$. In Fig. 6(b), derivatives of the two spin DOS in the ferromagnet near the Fermi energy are shown with a larger amplitude for spin-up

Fig. 6 Superconductor-ferromagnetic metal tunneling. **(a)** BCS density of states of a superconductor as a function of voltage in a magnetic field. **(b)** Temperature dependent kernels for each spin direction in the integral expressions for conductance. **(c)** Theoretical normalized conductance for each spin direction (dotted and dashed curves) and the total conductance (solid line).

Fig. 7 Cross section of an Al/Al$_2$O$_3$/Ag tunnel junction and plan view of a set of three junctions with contact pads.

electrons than for spin-down. The phenomenological theory states that the convolution of one spin function in Fig. 6(a) with the corresponding spin function in Fig. 6(b) gives the conductance at the voltage V shown in Fig. 6(c). The total conductance is given by the sum of the two spin contributions. In this figure, the voltage is measured from the Fermi energy of the ferromagnetic film. The fact that the inner peak at positive voltage is larger than the peak at the corresponding negative voltage indicates that electrons with their magnetic moments in the field direction (spin-up) predominate in the tunneling current.

We can do a quantitative analysis of the conductance curve to acquire the spin DOS of the superconducting film and the spin polarization of the tunneling current based on the previous two assumptions leading to Eq. (15). Referring to Fig. 6(c), if g(V) is the unsplit conductance function, we assume that ag(V-h) is the conductance contributed by the spin-up electrons shifted in voltage by the Zeeman splitting $h = \mu_B H / e$, and the

spin-down electrons have a contribution of (1-a)g(V+h). Here a is the fraction of spin-up electrons in the tunnel current. The total measured conductance G(V) is then the sum of the two spin contributions as is shown in Fig. 6(c) by the solid curve. For any value of V, four equations for the total measured conductance σ at points –V-h, -V+h, V-h and V+h in terms of the unsplit function g(x) can be written as

$$\sigma_1 = G(-V-h) = ag(-V) + (1-a)g(-V-2h) \qquad (17.1)$$

$$\sigma_2 = G(-V+h) = ag(-V+2h) + (1-a)g(-V) \qquad (17.2)$$

$$\sigma_3 = G(V-h) = ag(V) + (1-a)g(V-2h) \qquad (17.3)$$

$$\sigma_4 = G(V+h) = ag(V+2h) + (1-a)g(V) \qquad (17.4)$$

Assuming as in the microscopic theory that g(V)=g(-V) for the unsplit function, we obtain from Eqs. (17) the spin polarization P as a function of the measured conductances σ_1, σ_2, σ_3, and σ_4:

$$P = 2a - 1 = \frac{(\sigma_4 - \sigma_2) - (\sigma_1 - \sigma_3)}{(\sigma_4 - \sigma_2) + (\sigma_1 - \sigma_3)} \qquad (18)$$

From Eqs. (17.1) and (17.4), we can obtain the conductance of one spin orientation at any value of V in term of the quantity a and the measured total conductances G(V) and G(-V).

$$g(V-h) = [aG(-V) - (1-a)G(V)]/(2a-1) \qquad (19)$$

It appears from Eqs. (17) that any arbitrary value of voltage V and magnetic field could be selected to obtain P from Eqs. (17) and (18). In practice, how to choose the values of V and H are important as they determine the accuracy of the result. For very low values of H, the fringing field of the incompletely saturated magnetic film depairs the superconducting film and the small amount of splitting decreases the accuracy. On the other hand, for relatively large field H that is close to the critical field of the superconducting film, the depairing of the superconductor broadens the DOS curves and eventually obscures the effect of the magnetic field splitting. Values of V should be chosen so that σ_1, σ_2, σ_3, and σ_4 are close to the maxima of the conductance curves or at least in regions where the absolute values of the slope is small. This way the results will become much less sensitive to random experimental errors.

2.2.2   Experimental technique

There are two essential requirements for making the tunnel junctions: first, the barrier must be uniform and free from holes and is not too thick to allow tunneling. The tunneling thickness required is of the order of 1-2nm. Second, the surface quality of the superconductor must be good enough so that any undesirable surface conditions must extend much less than a coherence length into the superconductor.

These two problems can be solved most easily if the first-deposited electrode forms an oxide layer with a thickness suitable for tunneling. Al has been the most useful and reliable material because in addition to being uniform and pinhole-free, the oxide layer is chemically self-limiting in the tunneling thickness range. Sn, In and lead are also useful, although more difficult than Al. Compounds and alloys are more challenging because of their often short coherence lengths ($\leq$ 10nm), which impose severe demands on surface preparation.

Typical junction fabrication involves the following four steps [7]: first, an Al film is deposited through a shadow mask to form a long, narrow strip about 0.2mm wide. Next, the Al film is subject to an oxygen plasma to form a tunnel barrier. Then a counter-electrode material is evaporated through a mask to form a series of cross strips, making a number of junctions. The final step is to evaporate some material such as In solder or Au to form contact pads for attaching wires for electrical measurements. In many experiments, the Al film must be deposited on a substrate cooled to liquid-nitrogen temperature to make uniform and continuous 4 nm-thick films. Fig. 7 is a schematic of a tunnel junction.

Many tunneling results have been obtained with circuits measuring the derivative of I with respect to V, i.e. dI/dV as a function of V. The junction is biased with a voltage source that consists of a slow ramp and a small constant amplitude, audio frequency modulation. The AC current through the junction is measured using a lock-in detector. The output of the detector is then proportional to dI/dV.

2.2.3   Advantages and disadvantages

Spin-polarized tunneling from a ferromagnetic metal to a superconducting thin film provides a direct and powerful way to measure P of the FM. However, to get accurate results, the barrier and interface quality requirements are severe. Table 1 shows the increased value of measured P for some typical ferromagnets due to improvements in the junction structural quality.

Table 1   Tunnelling spin polarization obtained in experiments on FM/Al$_2$O$_3$/Al tunnel junctions [8]

FM	Ni	Co	Fe	Ni$_{80}$Fe$_{20}$	Ni$_{40}$Fe$_{60}$	Co$_{50}$Fe$_{50}$	Co$_{84}$Fe$_{16}$
P(%), old values[7]	23	35	40	32	–	–	–
P(%), new values[9,10]	33	42	45	48	55	55	55

2.3 Tunneling in a FM/I/FM junction-Julliere's model

Julliere's model [11] allows the calculation of spin polarization of a ferromagnet from the tunneling magnetoresistance (TMR) of a magnetic tunnel junction (MTJ).

2.3.1 Principle

A logical extension of the tunneling between ferromagnetic metals and superconductors is the tunneling between two ferromagnetic metals. It was reasoned that instead of using magnetic-field induced spin-split states of a superconductor as a spin detector, it is possible to use exchange-split states of another ferromagnet [8]. Such a structure, i.e. an $FM_1/I/FM_2$ junction is called a magnetic tunnel junction (MTJ). The most important property of an MTJ is that the tunneling current depends on the relative magnetization orientation of the two electrodes, which can be changed by an applied magnetic field. The tunneling current will be larger when the magnetization of the two metals are parallel than when they are antiparallel. This phenomenon is called tunneling magnetoresistance (TMR).

Julliere interpreted TMR in terms of a simple model based on two assumptions [8]. First, it is assumed that spin of electrons is conserved in the tunneling process. It follows, then, that tunneling of up- and down-spin electrons are two independent processes, so the conductance occurs in the two independent spin channels. According to this assumption, electrons originating from one spin state of the first ferromagnetic film are accepted by unfilled states of the same spin of the second film. If the two ferromagnetic films are magnetized parallel, the minority spins tunnel to the minority states and the majority spins tunnel to the majority states. If, however, the two films are magnetized

<div align="center">

PARALLEL ALLIGNM   **ANTIPARALLEL ALLIGNMENT**

Image removed due to
copyright considerations.

FM1 ^{I} **FM2**   **FM1** ^{I} **FM2**

</div>

Fig. 8 Schematic DOS diagram showing Julliere's assumption of spin conservation during tunneling

antiparallel, the majority spins of the first film tunnel to the minority states in the second film and vice versa as shown in Fig. 8.

Second, Julliere assumed that the conductance for a particular spin orientation is proportional to the product of the effective (tunneling) density of states (DOS) of the two ferromagnetic electrodes. According to these two assumptions, and following the analysis in much the same way as with tunneling between a ferromagnet and a superconductor,

the conductance for the parallel and antiparallel alignment, G_P and G_{AP}, can be written as follows:

$$G_P \propto N_1^{\uparrow} N_2^{\uparrow} + N_1^{\downarrow} N_2^{\downarrow} \propto a_1 a_2 + (1-a_1)(1-a_2) \qquad (20)$$

$$G_{AP} \propto N_1^{\uparrow} N_2^{\downarrow} + N_1^{\downarrow} N_2^{\uparrow} \propto a_1(1-a_2) + (1-a_1)a_2 \qquad (21)$$

where $N_i^{\uparrow}$ and $N_i^{\downarrow}$ are the tunneling DOS of the ferromagnetic electrodes (denoted by i=1,2) for the majority and minority spin electrons; a_1 and a_2 are the fractions of majority spin electrons in the DOS of the two ferromagnets. The subscripts P and AP indicate parallel and antiparallel magnetization. The TMR is defined as the conductance difference between parallel and antiparallel magnetizations, normalized by the antiparallel conductance:

$$TMR \equiv \frac{G_P - G_{AP}}{G_{AP}} = \frac{R_{AP} - R_P}{R_P} \qquad (22)$$

Using equations (20) and (21), we get Julliere's formula:

$$TMR = \frac{2P_1 P_2}{1 - P_1 P_2} \qquad (23)$$

which expresses TMR in terms of the effective P of the two FM electrodes:

$$P_i = \frac{N_i^{\uparrow} - N_i^{\downarrow}}{N_i^{\uparrow} + N_i^{\downarrow}} \qquad (24)$$

where i=1,2. Reformulating Eq. (24), we get

$$P_1 P_2 = \frac{TMR}{2 + TMR} \qquad (25)$$

If the P of one electrode, say, P_1, is known beforehand (e.g. through Tedrow-Meservey measurement), by measuring TMR, P_2 can be calculated from Eq. (25).

2.3.2 Experimental technique

Fig. 9 is a schematic of two MTJs fabricated in our lab. We prepare MTJs in much the same way as the fabrication of an S/I/FM junction introduced in section 2.2.2. First, a long vertical bottom electrode such as Co is deposited using e-beam evaporation through a shadow mask. Then a very thin Al layer (a few nm thick) is deposited at the liquid nitrogen temperature, followed by oxygen glow discharge to form the high quality tunnel barrier. Next, another ferromagnetic material is evaporated through a mask to from a series of cross strips, resulting in a number of junctions. A difference between the S/I/FM and FM1/I/FM2 fabrication is that in the latter, the insulating barrier material covers the whole area of the substrate, and is not defined as a long strip as in the former.

Measuring TMR is simple: when a voltage is applied between contacts 3 and 4 in Fig. 9, a current can be measured between contacts 1 and 2. Meanwhile, a magnetic field parallel to the film plane is swept from positive to negative values, maybe hundreds of orsteds, depending on the coercivity of the electrodes. Fig. 10 shows the experimental setup for
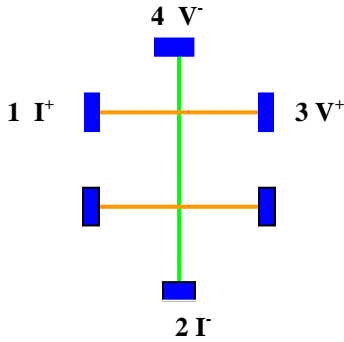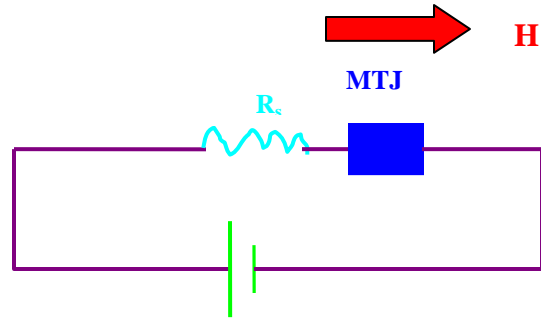
Fig. 9 Schematic of a MTJ

Fig. 10 Experimental setup to measure TMR

the measurement. R_s is a series resistor whose resistance is 1/5 to 5 times that of the tunneling junction. The TMR can be calculated per Eq. (22). If we know the P of one electrode beforehand, the P of the other electrode can be obtained from Eq. (25). Fig. 12 shows the first observation of reproducible, large magnetoresistance at room temperature by Moodera et al [12].

Image removed due to copyright considerations.

Fig. 12 The magnetoresistance in a CoFe/Al$_2$O$_3$/Co MTJ. The arrows indicate the relative magnetization orientation in the CoFe and Co layers (after [12]).

2.3.3 Advantages and disadvantages

Julliere's simple quantitative model has been used by many researchers to estimate the magnitude of TMR in MTJs from the known values of the spin polarization of ferromagnets obtained in experiments on FM/I/S tunnel junctions. It was also used to roughly estimate the P of a FM based on TMR values. E.g. Hu and Suzuki estimated the negative P of Fe_3O_4 from the TMR values of $Fe_3O_4/CoCr_2O_4/La_{0.7}Sr_{0.3}MnO_3$ MTJs [13]. But this model is too simple to describe all the experimental data. It assumes that the P of a tunneling current is solely determined by the P of the total electronic DOS of the ferromagnetic layers at the Fermi level. However, experimental results show that TMR strongly depends on the structural quality of the MTJ: improvements in the quality of the tunneling barrier layer and the interface between the insulating layer and the FM layer can enhance the measured value of TMR. Experiments also show that TMR also depends on the choice of the tunneling barrier.

2.4 Andreev reflection in a superconducting point contact

Andreev reflection at the interface between a superconductor and a ferromagnet metallic point contact has been attracting interest as a new technique to measure the spin polarization on ferromagnets because of its simplicity [1].

2.4.1 Principle

2.4.1.1 Andreev reflection

The conversion of a normal current to supercurrent at a metallic interface is called Andreev reflection, which is a well-known phenomenon in superconductivity. Fig. 13(A) shows the interface between a metal with P=0 and a superconductor. When an electron from the normal metal propagates toward the interface, for the electron to enter the superconducting condensate and proceed as part of the supercurrent, another electron from the metal is required to form a pair, thus leaving behind a hole at the interface. This hole has the opposite momentum of the incident electron and propagates away from the interface. The Andreev reflected holes act as a parallel conducting channel to the initial electron current, thereby doubling the normal-state conductance G_n (G=dI/dV) of the point contact for applied voltages eV<Δ, with Δ being half the superconducting gap at the interface. In an I-V measurement, the supercurrent conversion appears as an excess current added to the ohmic response at the interface. Fig. 13(B) illustrates the effect experimentally for a superconducting niobium point pressed into a Cu foil at a temperature of 1.6K. As can be seen, at low voltage, the normalized conductance is indeed twice that of the normal state and an excess current about 0.2mA is present.

Image removed due to
copyright considerations.

Fig. 13 Supercurrent conversion at the superconductor-metal interface for spin polarizations of *P*= 0 **and** *P* → 100%.

(**A**) Schematic of the process for *P*=0 when the Andreev reflection is unhindered by a spin minority population at E_F. The solid circles denote electrons and open circles denote holes.

(**B**) Experimental measurement of the *I-V* and differential conductance *dI/dV* at *T*=1.6 K via a superconducting Nb point contact on Cu. The vertical lines denote the bulk gap of Nb: Δ (*T*=0) =1.5 meV. The dashed line is the normal state *I-V* for a conductance of *Gn*= 0.194 ohm^{-1}.

(**C**) Schematic of process for *P*=100% when there is no supercurrent conversion at the interface.

(**D**) Experimental *I-V* and *dI/dV* at *T* =1.6 K via the Nb point contact on CrO$_2$. The dashed line is the normal state *I-V* for a conductance of *Gn*=0.417 ohm^{-1}.

2.4.1.2 Effect of spin polarization on Andreev reflection

Tracking the spin during Andreev reflection shows that the process is a coherent interspin-subband transfer that is sensitive to the relative electronic spin DOS or P of the normal metal at E_F. Let us look at Fig. 13(A) again. Because a superconducting pair consists of a spin-up and a spin-down electron, an incident spin-up electron in the metal requires a spin-down electron to be removed from the metal as well for conversion to supercurrent. The removal of the spin-down electron leaves a spin-up hole that is Andreev reflectd back into the metal. Since the spin-up hole is the absence of a spin-down electron, by convention, it is in the spin-down DOS as shown in Fig. 13(A). Whether and to what extent Andreev reflection is allowed depends on P. When P=0, Andreev reflection is not hindered by a lack of minority spin carriers for the formation of cooper pairs to enter supercurrent. However, in the case of P=100% near E_F as depicted in Fig. 13(C), there are no spin-down states in the normal metal to provide the other member of the superconducting pair for Andreev reflection. Supercurrent conversion via Andreev reflection is effectively blocked. As a result, only single particle excitation is allowed to contribute to the conductance. Because of the energy gap in the superconductor, for voltages eV<Δ, the single-particle states conductance is suppressed. Fig. 13(D) shows the result when a superconducting Nb point contact is placed on an epitaxial film of CrO$_2$, which is suggested to be a half-metal FM and have P=100% at E_F. The conductance curve directly confirms the 100% P because nearly all of the Andreev reflection has been suppressed, implying almost full spin polarization.

For intermediate spin polarizations, the Andreev reflection is partially blocked, because for an incident up-spin electron near E_F, there may or may not be a down-spin electron available for cooper pair formation. Soulen et al [1] adapted the Blonder-Tinkham-Klapwijk (BTK) theory for conventional Andreev reflection where P=0 to the case for spin-polarized materials (P $\neq$ 0) by decomposing the current into two parts: an unpolarized current I_{unpol} that carries no net P and obeys the conventional BTK theory and a polarized current I_{pol} that carries all of P and thus entirely a quasiparticle current. In the case of a ballistic point contact with no interfacial scattering (Z$\approx$0), for eV<<Δ and $K_B T$<<Δ, they arrived at the following equation which allows for easy determination of P from the conductance curve.

$$\frac{1}{G_n}\frac{dI}{dV}(eV \rightarrow 0, T \rightarrow 0; P, Z = 0) = 2(1 - P) \qquad (26)$$

When $Z \neq 0$ and T is finite, a numerical fitting procedure over the entire voltage range with their modified BTK model can be used to obtain P.

Fig. 14 shows a series of samples that have varying degrees of P, demonstrating the applicability of the superconducting point contact technique.
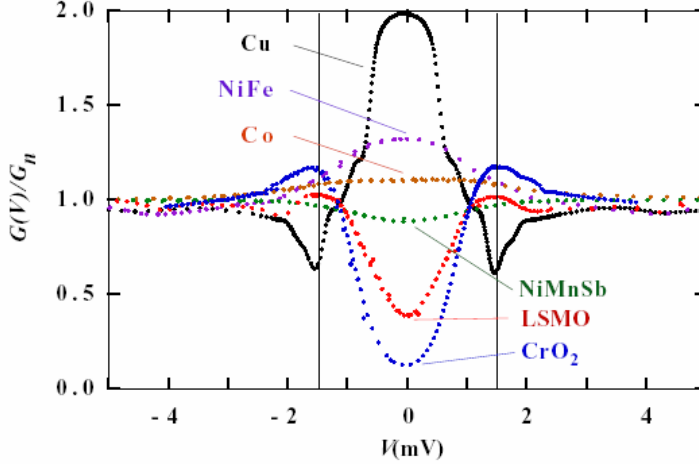

Fig. 14 The differential conductance for several spin-polarized metals showing the suppression of Andreev reflection with increasing *P*. The vertical lines denote the bulk gap of Nb: $\Delta (T=0)$=1.5 meV.

Soulen pointed out [1] that the P measured by the Andreev reflection (Pc) is defined differently from the Tedrow-Meservey results P_T, which is more accurately a tunneling polarization:

$$P_C = \frac{N_\uparrow(E_F)v_{F\uparrow} - N_\downarrow(E_F)v_{F\downarrow}}{N_\uparrow(E_F)v_{F\uparrow} + N_\downarrow(E_F)v_{F\downarrow}} = \frac{I_\uparrow - I_\downarrow}{I_\uparrow + I_\downarrow} \qquad (27)$$

$$P_T = \frac{N_\uparrow(E_F)|T_\uparrow|^2 - N_\downarrow(E_F)|T_\downarrow|^2}{N_\uparrow(E_F)|T_\uparrow|^2 + N_\downarrow(E_F)|T_\downarrow|^2} \qquad (28)$$

where $T_\uparrow$ and $T_\downarrow$ are spin dependent tunneling matrix elements. These matrix elements are determined by wave function overlap at the interface, and should therefore be different for the spin-up and spin-down bands. These different definitions may explain the discrepancy of P obtained by the two techniques.

2.4.2 Experimental technique

The probes for this technique were fabricated by mechanically polishing rods of superconducting material (Nb and Ta) to a cone-shaped sharp point of radius around 100 µm with progressively fine sand paper. The extreme portion of the tips was studded with several protrusions that were 1 µm or smaller which likely formed the actual point contact.

Positioning and adjustment of the point contact was achieved by mechanical means: the tip was attached to a drive shaft vertically positioned above the sample material. The shaft was driven by a micrometer mechanism capable of moving the point linearly by 100 μm per revolution.

Conventional four-terminal transport measurements were made with the point contact and sample immersed in a liquid He bath at either 4.2 or 1.6 K. The *dI/dV* data were obtained by standard ac lock-in techniques at a frequency of 2 kHz.

2.4.3   Advantages and disadvantages

Andreev reflection is a relatively new technique to measure spin polarization. The authors assert that [1] the advantage of Andreev reflection is its simplicity. Unlike Tedrow-Meservey method which has stringent requirement for an ultra thin uniform oxide layer, and thus may make the study of some interesting materials difficult, the superconducting point contact method requires no magnetic field and has no special constraints on a sample. Thin films, single crystals and foils of several metals have been successfully studied. Soulen et al were also able to measure a few compounds such as NiMnSb, LaSrMnO and CrO_2 that had not been examined by the tunnel junction technique.

Although there seems to be some rough correspondence between the results of Andreev reflection measurements and spin-polarized tunneling of the Tedrow-Meservy method, for some materials the discrepancy is huge. For example, Soulen et al measured a P of 37% for Ni, while the Tedrow-Meservy method gave a P=25%. Soulen et al attributed the difference to impurities and the different definitions of P.

Tsymbal et al [8] claimed that the relevance of Andreev reflection for MTJs and TMR values are questionable at best, and the rough correspondence between spin dependent tunneling across Al_2O_3 and Andreev reflection measurements are most probably spurious.

3   Conclusion

Measuring spin polarization of ferromagnetic materials easily and accurately is important for the advancement of spintronics. This paper reviews the four most commonly used methods for determining the degree of spin polarization in a ferromagnet. Through the discussions above, we have seen that each experimental technique has its own advantages and disadvantages. Because of the rather complicated equipment, spin-resolved photoemission is not often used to determine P. The Tedrow-Meservey method is a good alternative. Julliere model allows rough P estimation at high temperatures. Andreev reflection seems promising due to its not so severe requirement on sample preparation. Besides these four methods, there are still other techniques such as field emission that has not been pursued further since about 1980, electron capture spectroscopy, secondary electron emission, spin-polarized metastable-atom de-excitation spectroscopy, and Mössbauer spectroscopy, etc [4,6].

One should be careful when comparing P values measured using different techniques, and try to discern which kind of spin polarization they are measuring, P_N or P_{Nv}, etc.; whether they sample the localized electrons or highly itinerant states. Getting a definite answer can be challenging and sometimes requires demanding theoretical work and advanced experimental techniques.

References

[1] R. J. Soulen Jr., J. M. Byers, M.S. Osofsky, et al., Science, **282**, 85 (1998).
[2] I.I. Mazin, Phys. Rev. Lett. **83**, 1427(1999).
[3] G. Busch, M. Campagna, P. Cotti, et al, Phys. Rev. Lett. **22**, 597 (1969).
[4] R. Feder, ed. Polarized Electrons in Surface Physics, World Scientific,
      Singapore, 1985.
[5] D. J. Huang, C. F. Chang, J. Chen, et al, J. Magn. Magn. Matt., **239**, 261(2002).
[6] P. M. Tedrow, R. Meservey and P. Fulde, Phys. Rev. Lett. **25**, 1270 (1970).
[7] R. Meservey and P. M. Tedrow, Phys. Rep. **238**, 173 (1994).
[8] E. Y. Tsymbal, O. N. Mryasov, and P. R. LeClair, J. Phys: Condens. Matter, **15**,
     R109-R142 (2003).
[9]J. S. Moodera, J. Nassar, and G. Mathon, Annual Rev. Mater. Sci. **29**, 381(1999).
[10]D. J. Monsma, and S.S. P. Parkin, Appl. Phys. Lett. **77**, 720(2000).
[11] M. Julliere, Physics Letters, **54A**, 225 (1975).
[12] J. S. Moodera, L.R. Kinder, T. M. Wong and R. Meservey, Phys. Rev. Lett. **74**,
     3273(1995).
[13] G. Hu and Y. Suzuki, Phys. Rev. Lett. **89**, 276601(2002).